Ann. Phys. (Berlin) **527**, No. 9–10, 556–569 (2015) / DOI 10.1002/andp.201500144

annalen der physik

Original Paper

Vibrational relaxation and decoherence in structured environments: a numerical investigation

Matteo Bonfanti[1,*], *Keith H. Hughes*[2], *Irene Burghardt*[3], *and Rocco Martinazzo*[1,4,*]

Received 1 March 2015, revised 6 May 2015, accepted 15 June 2015
Published online 7 July 2015

Vibrational relaxation is a key issue in chemical reaction dynamics in condensed phase and at the gas-surface interface, where the environment is typically highly structured and cannot be expressed in terms of a simple friction coefficient. Rather, full knowledge of the coupling of the molecular oscillator to the environment is required, as typically subsumed in the spectral density of the environmental coupling. Here, we focus on harmonic Brownian motion and investigate the effectiveness of classical, canonical position autocorrelation functions to compute the spectral density of the coupling needed to describe vibrational relaxation in complex environments. Classical dynamics is performed on model systems, and several effects are investigated in detail, notably the presence of anharmonicity, the role of a high-frequency "Debye" cutoff in the environment and the influence of the detailed structure of the latter. The spectral densities are then used in standard independent oscillator Hamiltonian models which are numerically solved at $T = 0$ K to investigate quantum relaxation and decoherence.

1 Introduction

Vibrational relaxation plays a key role in many physical and chemical processes in condensed phases [1]. In activated barrier crossing, relaxation of reaction products has to be faster than re-crossing, thereby determining the reliability of transition-state approaches to reaction dynamics. Ground-state molecules that are photoexcited to an electronically excited state may undergo fast vibrational relaxation and get trapped into a local neighboring minimum of the excited-state potential, or start a fast, excited-state dynamics which ultimately leads to the photo-reaction products. Vibrationally excited molecules may store a comparatively large amount of energy and thus open non-thermal reaction pathways which would otherwise be impossible. Mode-selective chemistry has to compete with energy relaxation and re-distribution, conversely energy dissipation is a prerequisite for sticking of atoms and molecules to solid surfaces, *i.e.* for surface chemistry.

Modeling vibrational relaxation requires information on the relevant molecular vibrational degrees of freedom, and their coupling to the complicated environment in which they are placed. While the former are accurately described by many high-quality electronic structure methods available today, the latter is not always easily identifiable and, most often, is not in a form which is readily usable for high-dimensional quantum dynamics. The need of a quantum description arises since the vibrational energy is typically larger than thermal energy; a problem which forces one to deal with a quantum system interacting with a quantum bath which is typically highly structured.

Progress in the quantum description can be made with the Independent Oscillator (IO) model [1–5], since the latter provides a rather general representation of the system-bath dynamics and is particularly convenient for numerically exact simulations of the open system quantum dynamics. IO Hamiltonians can be managed with exact wavepacket techniques (including possibly Monte Carlo wavepacket sampling, for handling finite-temperature situations [6]) up to several tens of degrees of freedom [7–9]. Furthermore, detailed information on

* Corresponding authors E-mail: matteo.bonfanti@unimi.it; rocco.martinazzo@unimi.it
[1] Dipartimento di Chimica, Università degli Studi di Milano, v. Golgi 19, 20133 Milano, Italy
[2] School of Chemistry, Bangor University, Bangor, Gwynedd LL57 2UW, UK
[3] Institute of Physical and Theoretical Chemistry, Goethe University Frankfurt, Max-von-Laue-Str. 7, 60438 Frankfurt/Main, Germany
[4] Istituto di Scienze e Tecnologie Molecolari, Centro Nazionale Richerche, v. Golgi 19, 20133 Milano, Italy

the structure of the environment can easily be encoded in terms of bath oscillator frequencies and coupling parameters. However, a key problem is *obtaining* the spectral density (SD) function in the first place. If an analytical form of the total potential is known, the SD, $J_0(\omega)$, can be computed by a careful small amplitude expansion around the relevant global minimum. However, this may be a difficult task for a complex potential (*e.g.* when the separation between the system and the bath is not evident) or simply not possible in practice because the potential is not explicitly available, or the environment is dynamically evolving (*i.e.* well defined minima cannot be singled out). Nowadays, one most often accesses dynamical information *bypassing* the need of computing an accurate potential, *e.g.* using *on-the-fly* simulations such as *ab initio* molecular dynamics, and thus a method which uses only dynamics as an input is highly preferred. For a related discussion, see recent work of Ref. [10].

In the present work we describe and thoroughly check a procedure for computing the spectral density from molecular dynamics simulations. The approach makes use of analytical results which can be obtained for harmonic Brownian motion and its position (or velocity) autocorrelation function, and essentially inverts the latter to give $J_0(\omega)$. We test this approach on a variety of models and discuss its limits and its range of applicability.

Furthermore, since the ultimate goal is to address vibrational quantum dynamics, we also investigate vibrational relaxation and decoherence in the ensuing IO models, and show that they can be tackled with numerically exact methods, in a realistic range of parameters describing molecular systems and coupling to typical environments. Hence, we provide a full description of the procedure, from the classical equilibrium dynamics used to infer the environmental coupling to the quantum dynamics. We emphasize here that this article does *not* address the fundamental issue of whether and how a reduced dynamics can be exactly mapped into some sort of generalized Langevin equation (GLE) and corresponding IO model [11–13].

The paper is organized as follows. In Section 2, we sketch our approach and in Section 3 we describe the models and the methods used for the classical and the quantum dynamical simulations. In Section 4 we present our results, which are then discussed in Section 5. Finally Section 6 summarizes and concludes.

2 Theory

The spectral density (of the environmental coupling) [4, 5] $J_0(\omega)$ appears in the generalized Langevin equation for a Brownian degree of freedom s of mass m subjected to a deterministic potential V and a stochastic force ξ

$$m\ddot{s}(t) + m\int_{-\infty}^{+\infty} \gamma(t-\tau)\dot{s}(\tau)d\tau + V'(s(t)) = \xi(t) \tag{1}$$

$J_0(\omega)$ is related to the real part of the frequency-dependent memory kernel through $J_0(\omega) = m\omega\Re\tilde{\gamma}(\omega)$ where

$$\tilde{\gamma}(\omega) = \int_0^{\infty} \gamma(t)e^{i\omega t}dt \tag{2}$$

$J_0(\omega)$ fully determines $\tilde{\gamma}(\omega)$ by virtue of the Kramers-Kronig relations and the Gaussian stochastic process $\xi(t)$ by virtue of the fluctuation-dissipation (FD) theorem of the second kind. Specifically, if we define the symmetrized memory kernel $\kappa(t) = \gamma(|t|)$ (in such a way that $\gamma(t) = \Theta(t)\kappa(t)$), the following relations hold

$$\kappa(t) = \frac{2}{\pi m}\int_0^{+\infty} \frac{J_0(\omega)}{\omega}\cos(\omega t)d\omega \tag{3}$$

$$\langle\xi(t)\xi(0)\rangle = \frac{\hbar}{\pi}\int_{-\infty}^{+\infty} \frac{J_0(\omega)}{1-e^{-\hbar\beta\omega}}e^{-i\omega t}d\omega \tag{4}$$

Here the force correlator has been written for a quantum environment; the classical limit can be obtained at high temperatures ($\beta = \frac{1}{k_B T} \to 0$), where Eq. (4) reduces to the classical FD expression, $m\kappa(t)/\beta$.

For classical harmonic Brownian motion, $V = \frac{1}{2}m\omega_0^2 s^2$, the spectral density determines not only the correlation function of the environmental fluctuations according to Eq. (4), but also the frequency-dependent autocorrelation function of the position, $\tilde{C}(\omega) = \int_{-\infty}^{+\infty} e^{i\omega t}C(t)dt = \int_{-\infty}^{+\infty} e^{i\omega t}\langle s(t)s(0)\rangle dt$, namely through

$$\frac{1}{2}\omega\tilde{C}(\omega) = \frac{k_B T}{m}\Im\left(\frac{1}{\omega_0^2 - \omega^2 - i\omega\tilde{\gamma}(\omega)}\right) \tag{5}$$

which can be obtained by Eq. (1) upon performing a harmonic analysis of that equation and applying the FD theorem [14].

In general, for realistic systems, the autocorrelation function of the displacement $\langle s(t)s(0)\rangle$ (or, equivalently, of the velocity $\langle\dot{s}(t)\dot{s}(0)\rangle = -\frac{d^2}{dt^2}\langle s(t)s(0)\rangle$) is readily available from equilibrium classical simulations (or *ab initio* molecular dynamics calculations), and can be used to infer the coupling to the environment provided Eq. (5) can be "inverted" to give $J_0(\omega)$ in terms of $\tilde{C}(\omega)$. This can be accomplished by introducing the retarded correlation function $C^+(t) = \Theta(t)C(t)$ and exploiting the analytic properties of its Fourier transform (see Appendix A).

The result is

$$J_0(\omega) = \frac{k_B T}{2} \frac{\omega \tilde{C}(\omega)}{|\Gamma^+(\omega)|^2} \tag{6}$$

where $\Gamma^+(\omega) = \lim_{\epsilon \to 0^+} \Gamma(\omega + i\epsilon)$, and

$$\Gamma(z) = \frac{1}{\pi} \int_{-\infty}^{+\infty} \frac{\omega \tilde{C}(\omega)/2}{\omega - z} d\omega \tag{7}$$

is a "Cauchy transform" of the function $f(\omega) = \omega \tilde{C}(\omega)/2$. Eq. (6) is our working equation which translates dynamical information into a coupling strength. Related procedures for the Laplace inversion of the position autocorrelation function have been used, e.g., in Ref. [15] in a classical-mechanical context. In the following, we check numerically its performance using the model systems described below, but in general, classical atomistic simulations can be used to generate the dynamics of interest.

Once $J_0(\omega)$ is known it can be used to construct a quasi-equivalent Independent Oscillator (IO) (also known as Caldeira-Leggett) Hamiltonian [4, 5]

$$H^{IO} = \frac{p_s^2}{2m} + V(s) + \sum_{k=1}^{F} \left[\frac{p_k^2}{2\, m_k} + \frac{m_k \omega_k^2}{2} \left(x_k - \frac{c_k}{m_k \omega_k^2} s \right)^2 \right] \tag{8}$$

where the s degree of freedom is coupled to a collection of harmonic oscillators $(x_k,\ p_k)$ of mass m_k and frequency ω_k (in the following $m_k \equiv \mu$ for all k is used, where μ is a numerically convenient choice of the mass). To this end, the coupling coefficients and the bath frequencies need to sample the spectral density $J_0(\omega)$ of the problem, *e.g.* for evenly spaced frequencies $\omega_k = k\Delta\omega$ the coefficients are given by

$$c_k = \sqrt{\frac{2}{\pi} m_k \omega_k \Delta\omega\, J_0(\omega_k)} \tag{9}$$

The equivalence between the two dynamical formulations holds for finite times only, namely for times less than the Poincaré recurrence time $t_P = 2\pi/\Delta\omega$ of the finite system; the latter needs to be set larger than the time-scale of interest of the problem by choosing the appropriate number of oscillators in the spectral range of interest. In practice, this further implies the existence of a frequency cutoff ω_c which sets the shortest time that can be resolved $t_c = 2\pi/\omega_c$; higher frequencies, if present, can always be absorbed in a mass-renormalization term provided we are not interested in times smaller than t_c.

The Hamiltonian of Eq. (8) can be quantized by applying standard quantization rules and represents the quantum problem that we tackle here at $T = 0$ K with a Multi-Configuration Time-Dependent Hartree (MCTDH) expansion of the wavefunction [7, 8], following previous works on similar model systems [16–20]. Further developments involving transformation of the bath Hamiltonian into linear chain form [21–24] and its application to similar problems have been discussed elsewhere [25].

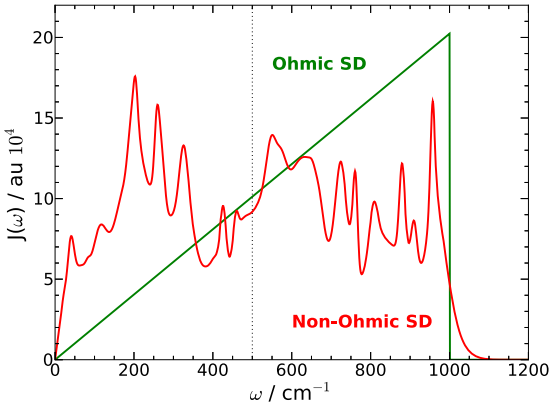

Figure 1 Model spectral densities adopted in this work. In green, the Ohmic spectral density corresponding to a relaxation rate of $\gamma^{-1} = 100$ fs. In red a non-Ohmic spectral density randomly generated on the same scale as the reference Ohmic SD (atomic units).

3 Models and methods

3.1 Models

In the following we apply Eq. (6) using dynamical information extracted from several model systems. The systems are defined by the IO Hamiltonian of Eq. (8), and make use of different system potentials and bath parameters.[1] Two different model baths were considered, both with a "Debye" cutoff frequency $\omega_D \approx 1000$ cm^{-1}. The Markovian limit was represented by a truncated-Ohmic bath, defined by $J_0(\omega) = \gamma m \omega$ for $\omega \leq \omega_D$ and zero otherwise. A non-Markovian model $J_0(\omega)$ was defined by generating 200 random Gaussian functions in the interval $[0, \omega_D]$, randomly choosing their widths in the 5 - 50 cm^{-1} range and fixing their intensity so that the integrated SD approximately equals the Ohmic reference SD. This random spectral density is plotted in Fig. 1, while all the parameters of the bath and the values adopted are listed in Table 1. Two different models were used for the system potential, a harmonic model with frequency ω_s, *i.e.*

[1] Below, we will also briefly consider lifting the assumption of a bilinear coupling model.

Table 1 Parameters of the Hamiltonian

Model Hamiltonian	Parameter	Value	
Harmonic Oscillator	mass (m)	1.0078	amu
	frequency (ω_s)	500/2500	cm^{-1}
Morse Oscillator	mass (m)	1.0078	amu
	frequency (ω_s)	500/2500	cm^{-1}
	well depth (D_e)	1.5	eV
	Morse α	0.5557	$Å^{-1}$
Ohmic Bath	mass (μ)	1.0000	amu
	number (F)	500/50	
	Debye freq (ω_D)	1000.	cm^{-1}
	relaxation time (γ^{-1})	100.0	fs
non-ohmic Bath	mass (μ)	1.0000	amu
	number (F)	500/50	
	Debye freq (ω_D)	1200.	cm^{-1}

$V(s) = \frac{1}{2} m\omega_s s^2$, and a Morse model

$$V(s) = D_e \left(\exp\left(-\alpha s\right) - 1\right)^2 \tag{10}$$

Here D_e is the well depth and α^{-1} its "width", both of which determine the system frequency $\omega_s = \alpha\sqrt{2D_e/m}$. In either case, two different values of ω_s were considered: one below the Debye cutoff frequency, $\omega_s = 500$ cm^{-1}, and one well above it, $\omega_s = 2500$ cm^{-1}. Other relevant parameters are given in Table 1.

Ideally, for the models considered here, application of Eq. (6) should give back the same spectral density used above for defining the couplings, provided the system trajectory remains well within the harmonic region of the system potential (*i.e.* the dynamics is performed at low enough T). In practice, however, as will be shown below, the (realistic) case where $\omega_s > \omega_D$ proves to be numerically challenging, because the $\delta-$peak in $\tilde{C}(\omega)$ which appears at ω_s necessarily broadens and this fact hides either anharmonic effects or artificial damping introduced in the dynamics.

3.2 Classical dynamics

For each of the two models above we computed the autocorrelation functions of the oscillator coordinate s by averaging a set of classical trajectories at a given temperature. These trajectories were obtained by sampling a set of initial conditions from a thermal distribution and propagating them in the microcanonical ensemble. Canonical sampling was achieved with the help of Langevin dynamics, integrated with a symplectic algorithm [26] at two different temperatures, 5 K and 300 K. The other relevant parameters for the Langevin propagation are reported in Table 2. For the microcanonical dynamics, we used a velocity-Verlet algorithm, with parameters also reported in Table 2.

Table 2 Parameters of the molecular dynamics simulations

Parameter	Value	
Nr of trajectories	100	
Temperature	5/300	K
Equilibration Δt	0.2	fs
Equilibration $\tau_{relax} = \gamma^{-1}$	10.0	fs
Equilibration time	200.0	ps
Propagation Δt	0.05	fs
Propagation time	100.0	ps
Time step of trajectory sampling	2.5	fs

The frequency dependent correlation function $\tilde{C}(\omega)$ was obtained with the help of the Wiener-Khinchin theorem

$$\tilde{C}(\omega) = \lim_{\mathcal{T}\to\infty} \frac{1}{\mathcal{T}} \langle |S_{\mathcal{T}}(\omega)|^2 \rangle \tag{11}$$

where $S_{\mathcal{T}}(\omega)$ is the finite-time Fourier transform of each realization of the system trajectory $s(t)$

$$S_{\mathcal{T}}(\omega) = \int_0^{\mathcal{T}} dt\, s(t)\, e^{i\omega t}$$

and the average is over the initial conditions. To smoothen the autocorrelation function resulting from our finite time propagations, we further applied a damping exponential factor in time, $\exp(-t/\tau)$, with $\tau = 1.0$ ps larger than any time-scale of interest here.

3.3 Quantum dynamics

Finally, in order to illustrate the implementation of the whole procedure, the Hamiltonian of Eq. (8) – as defined by the spectral densities computed from Eqs. (6) and (11) for the models described above – was used for studying vibrational relaxation and decoherence with fully

quantum methods. Quantum simulations were performed with the multi-configuration time-dependent Hartree (MCDTH) method, using the Heidelberg MCTDH package [8, 9, 27].

Although MCTDH is a powerful computational approach for quantum dynamics, the computational cost of the calculations limits the bath size to 50 oscillators. This number of oscillators corresponds to a recurrence time of 1390 fs for the ω_D =1200 cm^{-1} cutoff and 1668 fs for the ω_D =1000 cm^{-1} cutoff, which, for both cases is well above the relevant timings of the processes considered here. In the primitive discrete variable representation (DVR) grid, a Hermite basis set was chosen for all degrees of freedom, including 20 points for the system DOF and 6 for each of the bath DOF. The single particle schemes adopted vary according to the bath representation, but in general the system was represented with a single mode, and the bath degrees of freedom were divided into combined modes of five oscillators. The initial state was defined as a product of a wavefunction for the system and one for the bath. The bath component consisted of a product of the ground state functions of the harmonic oscillators, which is the exact ground state of the bath when coupling with the system is neglected. For the system part, a different wavefunction was used depending on the kind of simulation. In the case of vibrational relaxation, an initially excited state of the system potential was chosen and the relaxation dynamics was investigated by looking at the vibrator energy. In the case of decoherence, the initial state of the system was defined as a superposition of two spatially separated Gaussians. The coherence between these two Gaussian packets was analyzed by computing $\langle s|\rho|s'\rangle$, the coordinate representation of the reduced density matrix of the system $\rho = tr_{x_1 \ldots x_F}|\Psi\rangle\langle\Psi|$, where tr is the usual trace over the indicated degrees of freedom. The off-diagonal elements of $\langle s|\rho|s'\rangle$ describe the spatial coherence of the two Gaussians and decay in time due to the interaction with the bath.

4 Results

When combining the model environments introduced above with the system potential parameters four main possibilities arise, depending on whether the oscillator frequency ω_s is larger or smaller than the bath Debye frequency ω_D ("High" and "Low" frequency cases, in the following, or "HF" and "LF" in short), and on whether the bath is Ohmic or not ("Ohmic" and "non-Ohmic"). For each of these possibilities, the system oscillator may be harmonic (HO) or anharmonic of Morse (MO) type.

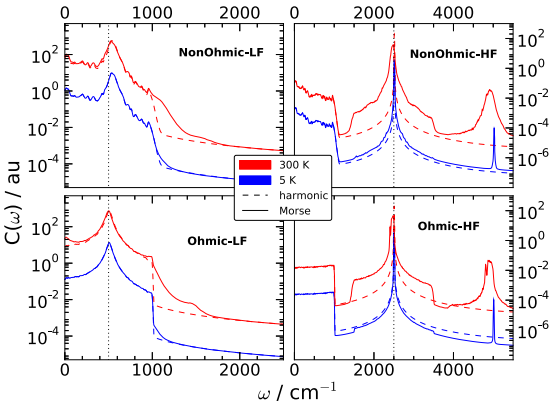

Figure 2 Frequency-dependent autocorrelation functions of the system coordinate $\tilde{C}(\omega)$ (atomic units) as obtained from classical simulations sampling different canonical equilibrium ensembles, blue for $T = 5$ K and red for $T = 300$ K. The different panels refer to the models considered (Ohmic-LF/HF and non-Ohmic-LF/HF, from bottom to top and from left to right; see text for details). Dashed (solid) lines for the harmonic (Morse) oscillator, whose central frequency ω_s is marked with the dashed vertical bar.

4.1 Spectral Density

The classical autocorrelation function of the system coordinate and its Fourier transform $\tilde{C}(\omega)$, were computed using the methodology explained in Section 3. For the different models considered, Fig. 2 depicts $\tilde{C}(\omega)$. As expected, the autocorrelation function scales linearly with the temperature T (see Eq. (5) for the Harmonic Brownian dynamics), but only approximately for the Morse oscillator, because of an additional broadening of the signal which depends on the temperature. Apart from this, the details of the spectra can be easily understood in terms of the oscillations of the system at its natural frequency ω_s and their coupling with the bath.

When the oscillator frequency lies *within* the spectral range of the bath ("LF" cases), the spectrum has a single band which arises from the superposition of the ω_s = 500 cm^{-1} system peak and the bath signal. For frequency larger than the bath cutoff ω_D, the band sharply decays. Anharmonic effects introduce a broadening of the spectrum which is larger as the temperature increases; hence at high temperature a much slower decay of $C(\omega)$ is found.

However, when the oscillator frequency lies *above* the bath spectral range ("HF" cases), there is a clear separation between the peak of the system and the band of the bath. Furthermore, the shape of the latter is almost independent of the system, *i.e.* whether it is harmonic or anharmonic. For the system, the HO case fea-

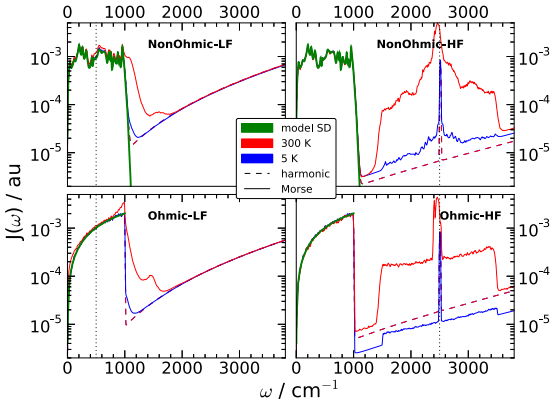

Figure 3 The spectral densities (atomic units) obtained by "inverting" the dynamical information of Fig. 2 (color coded as in that figure) are compared to the original ones used to define the models (green lines).

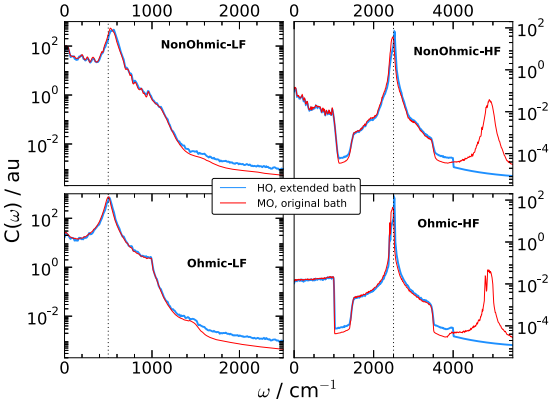

Figure 4 Frequency-dependent autocorrelation functions computed at 300 K for a HO system using the spectral densities obtained at the same temperature from the MO simulations. Blue lines for the HO results and red lines for the original MO ones.

tures a single Lorentzian peak (robust against variations of the bath and/or the temperature) which is the numerical representation of a $\delta-$Dirac contribution, as expected from Eq. (5) when ω_s lies outside the support of $J_0(\omega)$. Anharmonicity has two strong effects: on one hand it causes the appearance of a higher harmonic of the oscillator at a frequency $\omega = 2\omega_s$ =5000 cm^{-1}, on the other hand it induces a broadening of the $\delta-$Dirac signal that is about twice as large as the spectral width of the bath.

Next, we used the transformation of Eq. (6) and extracted the spectral density of the environmental coupling from the dynamical information contained in $\tilde{C}(\omega)$. Since the underlying dynamical models are always of the IO type - in which $J_0(\omega)$ was explicitly defined - we are able to thoroughly test our methodology by comparing the original spectral density with the one obtained by "inverting" the autocorrelation function. All these functions are plotted in Fig. 3. Several things are worth noticing.

When the system is HO, the transformation *perfectly* recovers the original spectral density up to the bath Debye frequency, irrespective of the temperature and of the model bath. For higher frequencies, the spectrum is not identically zero and shows an increasing baseline that is due to the numerical implementation of the Cauchy transform of Eq. (7), which used an unbiased cutoff frequency well above the spectral range of interest (ω_c = 4000 cm^{-1}). However, this problem could be easily amended here by setting ω_c equal to the bath Debye frequency. On the other hand, applying blindly the transformation of Eq. (6) when the system frequency is larger than ω_D, a sharp peak appears for $\omega \sim \omega_s$ which is the remnant of the numerical realization of the $\delta-$Dirac contribution mentioned above. A fictitious coupling to the bath appears here because numerically the autocorrelation function needs to be damped.

System anharmonicity introduces further complicating issues, as can be seen from the dramatic effect that the temperature has on the computed spectral density. At low T, the results are consistent with the harmonic case. At "high" temperature, and in contrast to the HO case, the remnant of the $\delta-$peak undergoes substantial broadening, as can be seen from the shape of the computed spectral density around ω_s (notice though that $J_0(\omega)$ is given on a logarithmic scale in Fig. 3). On close inspection the region most sensitive to the temperature extends to $\omega_s \pm \omega_D$ and the shape of the computed $J_0(\omega)$ in this region is reminiscent of mode combinations $\omega_s \pm \omega_k$ between the system frequency ω_s and the frequency of the bath oscillators ω_k. This is reasonable since the inversion procedure of Eq. (6) was designed for a harmonic system, and is here applied to an anharmonic system. Obviously, such temperature-dependent background in $J_0(\omega)$ is *unphysical* and reflects just the anharmonicity in the *system* potential which can always be included in the IO models used for the quantum simulations, without any additional cost.

Interestingly, the above results suggest that anharmonic effects of the systems can be effectively incorporated in the bath. We checked this by computing the correlation functions using the HO system model in conjunction with the spectral densities obtained from the MO models. As shown in Fig. 4, such correlation functions are in remarkable agreement with the original ones

obtained for the MO [2], thereby suggesting that the transformation of Eq. (6) establishes a map between an anharmonic system and a harmonic one, by "moving" the anharmonic effects from the system to the bath. The price to pay for this suggestive transformation is of course a temperature-dependent spectral density.

From a general perspective this empirical observation follows from the possibility of projecting out the system dynamics and describing it by means of a generalized Langevin equation [11, 12]. When employing Mori's projection operators this mapping is *exact* for arbitrary systems and provides a Brownian oscillator model with an effective, temperature-dependent frequency and memory kernel; here, the temperature dependence of the frequency is minimal.

4.2 Quantum Dynamics

The IO models were also used to investigate vibrational relaxation, as an illustration of what can currently be done for the quantum dynamics once a potentially complicated environment is replaced by a spectral density. The quantum simulations to be discussed here were performed by evolving in time a high-dimensional wavepacket which represents a $T = 0$ K situation, but extensions to finite temperatures are possible, *e.g.* with a Monte Carlo sampling of the appropriate initial-state wavefunction [6]. Details of the numerics were given in Section 3.

Results for the system energy decay are reported in Fig. 5 for the two interesting (fast) processes in which the molecular frequency ω_s lies within the Debye limit. Several different initial states were considered, as evident from the value of the energy at initial time, as well as the two model spectral densities described above (Ohmic and non-Ohmic for bottom and top panel, respectively). The energy given in Fig. 5 is the expectation value of the system Hamiltonian *plus* half the interaction energy, to account for the energy that at any time is in the coupling term; the adopted equal splitting of the coupling may be justified with the help of the virial theorem [17].

As depicted in Fig. 5, relaxation proceeds in few hundreds of fs, regardless of the initial state; in contrast, no relaxation is found on the same time-scale for the case $\omega_s > \omega_D$ (not shown). Results are given only for the Morse oscillator, but the harmonic oscillator behaves

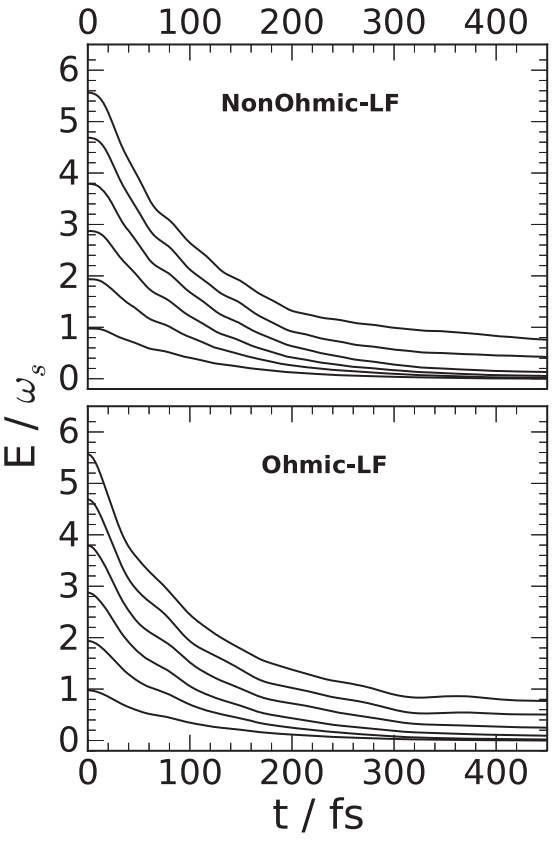

Figure 5 Time evolution of the system energy (as defined in the main text) for relaxation from different ν states. Average energies (in units of ω_s) are given for the low-frequency $\omega_s = 500$ cm^{-1} Morse oscillator coupled to an Ohmic (bottom) or to a non-Ohmic (top) bath.

very similarly, the main difference being only the value of the initial energy which reflects the influence of the anharmonic effects in the molecular spectrum. More interestingly, the relaxation rates are very similar for the two bath models, and no pronounced feature due to the structured environment is found. The reason for this behavior is that with the chosen coupling strength the width of the vibrational resonances is still relatively small that the system dynamics has no chance to sample the spectral density. Indeed, the effective relaxation time $\gamma_{eff}^{-1} = m\omega_s / J_0(\omega_s)$ for the non-Ohmic model is close to γ^{-1} =100 fs appropriate for the Ohmic bath (in line with the observed energy decay rates), and corresponds to $\delta\omega \sim 60\,\text{cm}^{-1}$, a value too small to provide detectable signatures of non-Markovian dynamics. This is confirmed by the distribution of the system energy into the bath oscillators, as provided by the evolution of their average occupation numbers shown in Fig. 6. This figure shows that energy exchange takes place almost entirely between the

[2] The absence of the highest frequency peak is only due to the fact that a smaller value of the cutoff was used in the Eq. (6), namely $\omega_c = 4000\,\text{cm}^{-1}$.

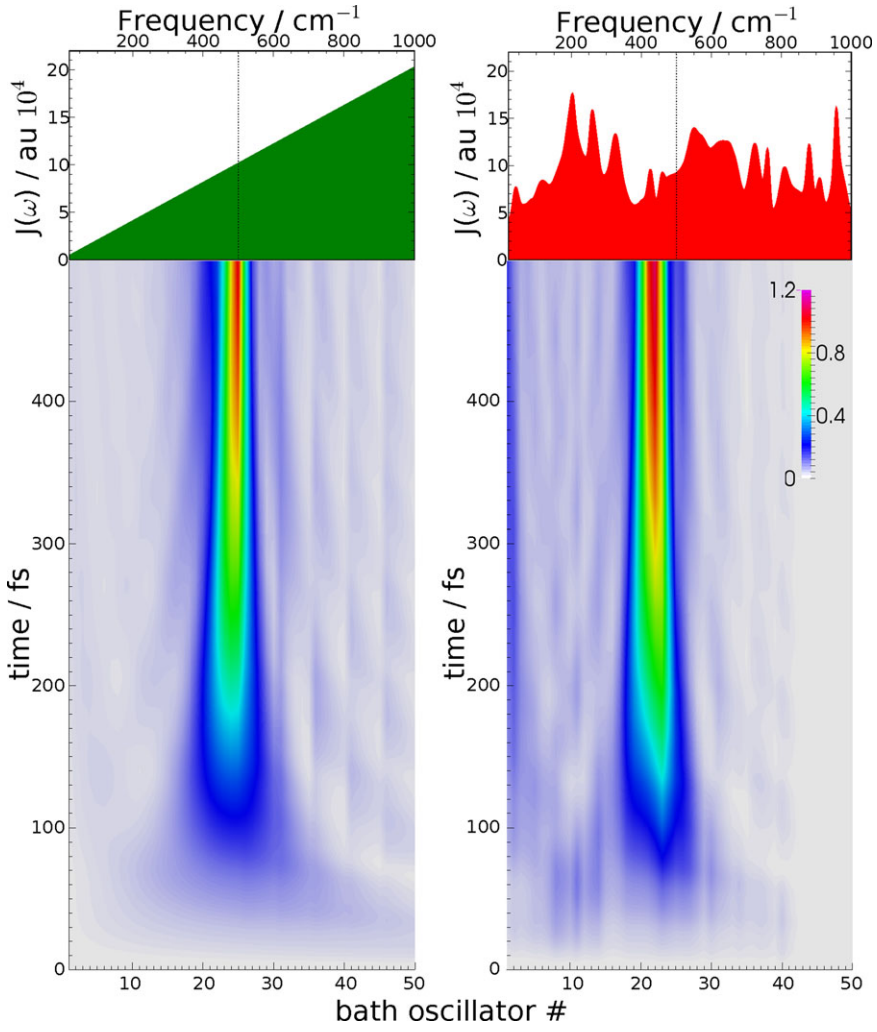

Figure 6 Time evolution of the average excitation number of the bath oscillators during relaxation of the $v = 5$ vibrational state of the Morse potential with $\omega_s = 500$ cm^{-1}. Left and right panels for the Ohmic and non Ohmic baths.

system and the few quasi-resonant oscillators, and that the coupling at $\omega = \omega_s$ =500 cm^{-1} has the same value for both the spectral densities.

Finally, the loss of coherence of the wavepacket as induced by the interaction with the environment was also investigated, following the same approach used in Ref. [18]. The initial wavefunction for the system was a sum of two Gaussians, symmetrically placed around the minimum of the potential at a distance of 1.8 a_0 for ω_s = 500 cm^{-1} and 0.8 a_0 for ω_s = 2500 cm^{-1}; the bath was taken in its ground-state, as above. Figure 7 illustrates the system reduced density matrix $\rho(s', s) = \langle s'|\rho|s\rangle$ at the beginning of the simulation, and after one, two and three vibrational periods T_{vib}; results are shown for the low-frequency harmonic oscillator (T_s =66.7 fs), but similar results were obtained for the Morse oscillator at the same frequency. In Fig. 7, on the diagonal $s = s'$, $\rho(s, s)$ represents a bimodal probability distribution for the s coordinate, with two distinct peaks that tend to merge on the time scale of vibrational relaxation. On a much shorter time scale, however, Fig. 7 shows the disappearance of the off diagonal peaks, describing the coherence between the two Gaussian states. Disappearance is complete in less than one vibrational period, in accordance with the much faster decoherence rate γ_{dec}. As shown in Ref. [18], in the Markovian regime at $T = 0$ K, $\gamma_{dec} = \Lambda_{dec}\gamma$, where the "decoherence factor" $\Lambda_{dec} = \frac{m\omega_s\delta^2}{2\hbar}$ depends on the mass and the frequency of the system, as well as on δ, which is a characteristic length scale of the problem, here the spatial separation between the Gaussians.

To quantify decoherence, and compare the different situations considered, we computed the coherence norm considered in Ref. [18], by running independent calculations for the $\pm$ combinations of the Gaussians. The results are depicted in Fig. 8, for all possible combinations

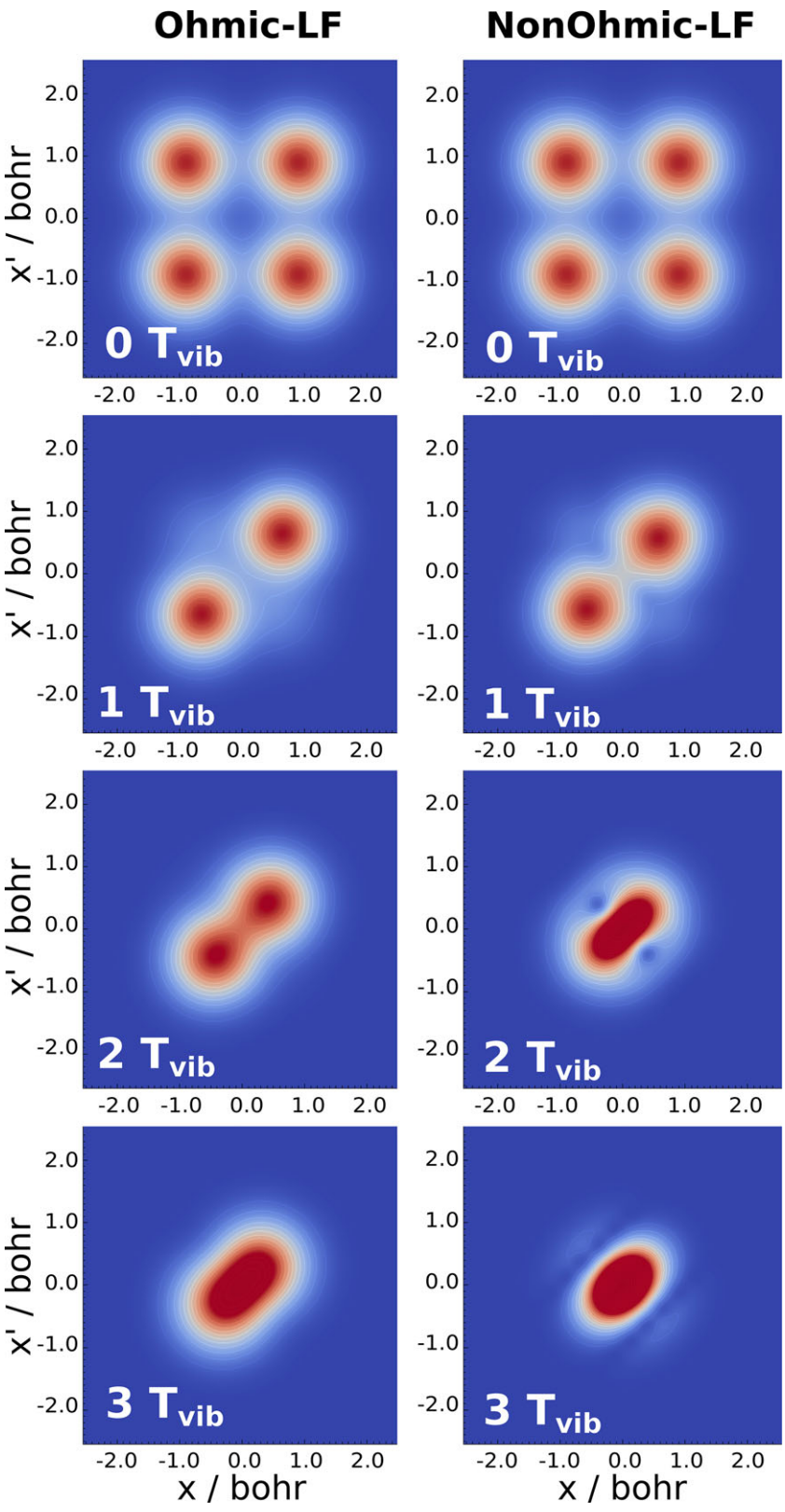

Figure 7 Contour map of the magnitude of the reduced density matrix of the system $\rho(s', s) = \langle s'|\rho|s\rangle$ during a relaxation dynamics. The initial state of the system was a superposition of two Gaussians, symmetrically placed around the minimum of the potential, 1.8 a_0 apart from each other. The system was HO with $\omega_s = 500$ cm^{-1}, and the bath was Ohmic in the left panels and non-Ohmic in the right panels. Results at initial time and after one, two and three vibrational periods T_{vib} (from top to bottom).

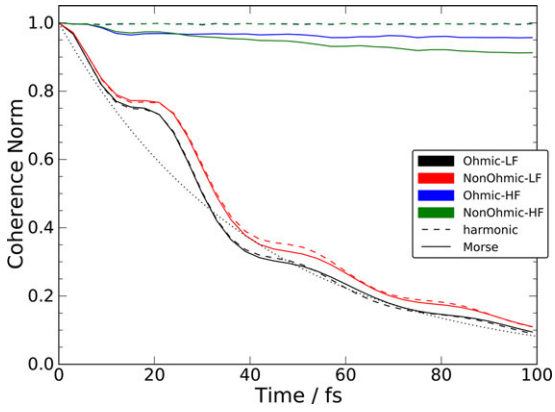

Figure 8 Coherence norm during the relaxation dynamics of the superposition of two Gaussians symmetrically placed around the minimum of the potential. The initial distance between the wavepackets was set in such a way that a decoherence factor $\Lambda_{dec} = 10$ results in the Markovian regime at $T = 0$ K. Also given, for comparison, the ideal decoherence rate in Markovian regime at $T = 0$ K, when $\gamma_{dec} = 10\gamma = 0.1$ fs^{-1} (dotted line).

of model environments and system potentials and with initial state parameters chosen in such a way that $\Lambda_{dec} = 10$ always holds. As can be seen from that Figure, and as could be expected on general grounds, only the low frequency cases ($\omega_s < \omega_D$) show appreciable decoherence. However, a surprising observation is that the behavior of the system is essentially the same, irrespective of the details of the bath: the deviations from the "ideal" exponential decay of the norm are similar for the Ohmic and non-Ohmic models, and likely relates only to the bath Debye cutoff ($\omega_D \approx 1000$ cm^{-1} for both models, corresponding to $t_D = 2\pi/\omega_D \approx 33$ fs).

5 Discussion

We have seen in the previous Section that the "inversion" procedure used to recover the spectral density is remarkably accurate for frequencies smaller than the Debye frequency of the bath. Noise at higher frequencies appears when $\omega_s > \omega_D$ and, in the bilinear coupling model, reflects just a numerically broadened $\delta-$peak in $\tilde{C}(\omega)$. Anharmonicity introduces further dynamical effects which should not be associated with the bath: the apparent higher cutoff in the LF simulations or the diffuse background found in the HF cases do not correspond to any true physical property of the bath. They are markedly temperature dependent –a clear-cut criterion for distinguishing these features from true features of the bath– hence the need to minimize the temperature used in the simulation. Notice that system anharmonic effects pose no real problems to modeling, as they are easily introduced in the working IO models by selecting the correct system potential.

In realistic situations, however, structures in the spectral region $\omega > \omega_D$ are expected quite generally from the failure of the bilinear coupling model when $\omega_s > \omega_D$. In such cases the coupling at frequencies beyond the Debye limit does have a physical origin, and thus the question arises whether $J_0(\omega)$ at such frequencies can be a surrogate for a more complicated coupling model, a rather intricate issue related to the general problem of whether a mapping of the system dynamics to a GLE exists and how it can be realized in practice (see *e.g.* Ref. [13] for a recent, in-depth analysis of this issue, and Appendix A for a connection to the present work). In general, real molecular oscillators are not harmonic and the system-bath coupling is not bilinear -especially if highly excited vibrational states are being probed- two factors which are hard to disentangle in finite-temperature cases where non-linearities in the coupling may be more marked (and more interesting). In such cases the present "dynamical" approach, when considered in the low-T limit above, can only provide the small-amplitude expansion of the coupling term and needs to be integrated with some empirical knowledge about the interaction between the molecular vibration and the environment.

For instance, a shape function $f(s)$ with the property $f(s) \approx s$ for $s \approx 0$, can be used to modulate the strength of the coupling to the bath depending on the system position s and in a way that is consistent with the bilinear coupling model where $f(s) \equiv$ s. Such function alone produces state-dependent friction, and seems to be a necessary (and simple) modification to address realistic situations; for instance, if s is the height of an adsorbate above a surface, the coupling should *vanish* for large s and be exponentially increasing for small s.

As for the bath, on the other hand, an exponential interaction model seems to be appropriate in typical situations where vibrational relaxation occurs, *i.e.* as a consequence of close encounters between the molecular vibrator and the atoms/molecules making up the environment. One simple *ansatz* of this kind, for instance, is the replacement of the term $s\sum_k c_k x_k$ in Eq. (8) with

$$\bar{D}e^{\alpha\bar{X}}\frac{e^{\alpha\bar{X}}-1}{\alpha}s$$

which can be justified in the context of a linear-chain representation of the bath (see Appendix B). Here $\bar{X}$ is the first effective mode of the linear-chain representation of the bath, $\bar{D}$ its coupling coefficient to the

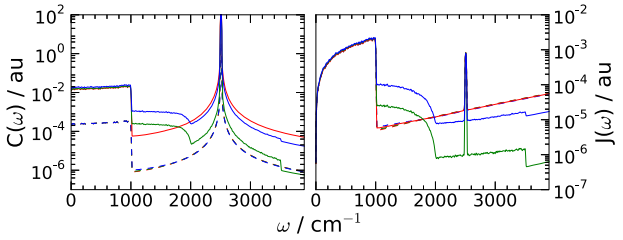

Figure 9 Left: frequency dependent position autocorrelation function for a high-frequency harmonic oscillator (ω_s =2500 cm^{-1} > ω_D) coupled to an Ohmic bath *via* a non-linear interaction term. Dashed and solid lines for $T = 5$ and 300 K, respectively, and red, green and blue lines for different values of the characteristic length parameter, α^{-1} =10, 2, and and 1.0 Å. Right: "effective" spectral densities obtained by using the results of the left panels as input.

system, α^{-1} a characteristic length of the interaction and $\bar{D}\bar{X} \equiv \sum_k c_k x_k$ by construction [21–24].[3] Such exponential interaction model makes use of the spectral properties of the proper bath (*i.e.* for frequencies $\omega < \omega_D$) to introduce multiphonon relaxing pathways already at the lowest order in perturbation theory, and is simple enough to be easily handled with the MCTDH method used above, provided the bath is first transformed in order to introduce its first effective mode X and its residual counterpart. Notice though that relaxation at such frequencies is slow enough that a master equation based on Fermi-golden rule state-to-state rates should suffice in most cases; with the coupling above, the necessary thermal rates k_{ji} can be obtained analytically [1], and only need the characteristic length α^{-1} and the spectral density $J_0(\omega)$ as inputs.

We checked the influence that the above non-linear interaction term has on the classical results, by computing the system autocorrelation function of the position in the simplest case, *i.e.* the harmonic oscillator with a frequency higher than the Debye cutoff, for several values of the characteristic length α^{-1}. The results of such simulations are reported in Fig. 9, where a structure for $\omega > \omega_D$ appears at high temperatures which can be clearly assigned to non-linearities in the interactions.

6 Conclusions

In this work the effectiveness of the position (or velocity) autocorrelation functions of bound systems in computing the spectral density of the environmental coupling needed to describe relaxation and decoherence of molecular vibrations in a condensed phase environment was investigated. Although applied to relatively simple models, the proposed approach has been shown to be robust and accurate for proper frequencies of the bath (i.e. $\omega < \omega_D$). At higher frequencies, effects from the anharmonicity in the system potential and/or non-linearities in the coupling have been identified and discussed in detail, and a simple extension to non-linear coupling models was suggested. Finally, quantum dynamics has been shown to be feasible to address vibrational relaxation and decoherence. Work is in progress to investigate such issues in realistic "molecular" systems comprising real molecular oscillators coupled to complicated environments.

Appendix A: Derivation of Eq. (6)

In this Appendix a derivation of Eq. (6) is given based on the analytic properties of the Fourier-Laplace transform of the retarded correlation function $C^+(t) = \Theta(t)C(t)$. The same results follow with the help of Laplace transforms. Let $\hat{C}(z) = \int_{-\infty}^{+\infty} e^{izt} C^+(t)dt$ ($\Im z > 0$) be the Fourier-Laplace transform of $C^+(t)$ and $\hat{C}^+(\omega) = \lim_{\epsilon\to 0} \hat{C}(z)$ its limit on the real axis, satisfying $2\Re\hat{C}^+(\omega) = \tilde{C}(\omega) = \tilde{C}^*(\omega) = \tilde{C}(-\omega)$ where $\tilde{C}(\omega)$ is the ordinary Fourier transform of $C(t)$. In the following we make use of the dispersion relation in the form

$$f(z) - f_\infty = \frac{1}{\pi}\int_{-\infty}^{+\infty} \frac{\Im f(\omega) - \Im f_\infty}{\omega - z} d\omega$$

which is valid for any function which is analytic in the upper half complex plane (u.h.p.), $\Im z > 0$. We put $f(z) = iz\hat{C}(z)$, for which $f_\infty = -C(0) = -\int_{-\infty}^{+\infty} C(t)dt$, as it follows from Cauchy theorem in the u.h.p.

$$c = \frac{i}{\pi}\int_{-\infty}^{+\infty} \hat{C}^+(\omega)d\omega \equiv \frac{i}{2\pi}\int_{-\infty}^{+\infty} \tilde{C}(\omega)d\omega = iC(0)$$

(notice that the imaginary part of $\hat{C}^+(\omega)$ is odd). Hence,

$$\Gamma(z) = f(z) + C(0) = \frac{1}{\pi}\int_{-\infty}^{+\infty} \frac{\omega\tilde{C}(\omega)/2}{\omega - z} d\omega$$

The integrand can be re-written with the help of Eq. (5), thereby introducing the function $(\omega_0^2 - \omega^2 - i\omega\tilde{\gamma}(\omega))^{-1}$ which can be analytically continued in the u.h.p.[4] It thus

[3] In Refs. [23, 24] X and D were introduced in a mass-scaled form, *i.e.* $X = \sqrt{\mu}\bar{X}$ and $\bar{D} = D\sqrt{\mu}$, where μ is a typical mass for the environment.

[4] Notice that $\omega_0^2 - z^2 - iz\tilde{\gamma}(z)$ cannot vanish in the upper half plane. This is evident in the IO (equivalent) representation of the

follows

$$\Gamma(z) = \frac{k_B T}{m} \frac{1}{\omega_0^2 - z^2 - iz\tilde{\gamma}(z)}$$

Solving for $iz\tilde{\gamma}(z)$ and taking the imaginary part of the resulting expression for $z = \omega + i\epsilon$, $\epsilon \to 0^+$, we obtain the desired result

$$J_0(\omega) = k_B T \frac{\Im S^+(\omega)}{|\Gamma^+(\omega)|^2} = \frac{k_B T}{2} \frac{\omega \tilde{C}(\omega)}{|\Gamma^+(\omega)|^2}$$

Notice that for $z = 0$, it also follows

$$\Gamma(0) = C(0) \equiv \langle s^2 \rangle = \frac{k_B T}{m} \frac{1}{\omega_0^2}$$

which is the classical equipartition theorem, as it should be from the FD theorem.

To establish the connection with more general approaches using two correlation functions (see *e.g.* Ref. [13]), we start from the following form of the GLE

$$\dot{p}(t) + \int_0^{+\infty} \gamma(t-\tau)\, p(\tau) d\tau - F(t) = \xi(t)$$

where the initial time has been reset to $t = 0$ and the conservative force $F(s) = -V'(s)$ has been introduced. It follows that the following relation holds between the momentum-momentum ($C_{pp}(t)$) and force-momentum ($C_{Fp}(t)$) correlation functions

$$\dot{C}_{pp}(t) = C_{Fp}(t) - \int_0^{\infty} \gamma(t-\tau) C_{pp}(\tau) d\tau$$

Hence, introducing the retarded correlation functions $C^+_{XY}(t) = \Theta(t) C_{XY}(t)$ for $X = p, F$ and $Y = p$ and noticing that $\int_0^{\infty} e^{i\omega t} \dot{C}_{pp}(t) dt = -C_{pp}(0) - i\omega \hat{C}^+_{pp}(\omega)$ we obtain the frequency-dependent memory kernel in terms of the above two correlation functions

$$\tilde{\gamma}(\omega) = \frac{\hat{C}^+_{Fp}(\omega) + C_{pp}(0)}{\hat{C}^+_{pp}(\omega)} + i\omega$$

For Harmonic Brownian motion $C_{pp}(t)$ and $C_{Fp}(t)$ are mutually dependent

$$\frac{dC_{Fp}(t)}{dt} = -\omega_0^2 C_{pp}(t)$$

(where ω_0 is the system frequency), and the Langevin equation for the correlation functions can be re-written as

$$\ddot{C}_{pp}(t) = -\omega_0^2 C_{pp}(t) - \int_0^{\infty} \frac{d\gamma(t-\tau)}{dt} C_{pp}(\tau) d\tau$$

and Fourier-Laplace transformed to give

$$\hat{C}^+_{pp}(\omega) = \frac{i\omega C_{pp}(0)}{\omega^2 - \omega_0^2 + i\omega\tilde{\gamma}(\omega)}$$

Equivalently, in terms of the frequency-dependent position autocorrelation function $\hat{C}^+(\omega)$ introduced in the main text

$$i\omega \hat{C}^+(\omega) + C(0) = \frac{k_B T}{m} \frac{1}{\omega^2 - \omega_0^2 - i\omega\tilde{\gamma}(\omega)}$$

where $\hat{C}^+_{pp}(\omega) = m^2(-i\omega C(0) + \omega^2 \hat{C}^+(\omega))$ has been used and thermal equilibrium conditions assumed to hold at $t = 0$ ($C_{pp}(0) = mk_B T$). When analytically continued in the upper half plane this expression is just the equation obtained above for the function $\Gamma(z)$.

In closing this Appendix we compare the approach we used in the main text with the two-correlation function approach described above. The first uses a single correlation function and requires no *a priori* knowledge of the system potential; the latter, on the other hand, proves to be a general, *exact* method to extract the memory kernel *provided the system dynamics can be exactly mapped to a GLE*. Two cases are typically discussed. The first occurs when Mori's linear projector operators are used to exactly map the reduced system dynamics into an effective (temperature-dependent) Brownian harmonic system; the second when the Hamiltonian is of the IO-type (Eq. (8)) with an arbitrary system potential. In the first case, the standard, Mori-projected GLE equation for the system coordinate is exact for arbitrary systems but inherently linear, and cannot be used to describe nonlinearities (*i.e.* only dynamical variables which lie in the Hilbert subspace spanned by s and p_s are guaranteed to be correctly reproduced). At low temperature the Mori-projected GLE (and its memory kernel) reduces to the GLE for a Brownian HO used in the main text, provided the system has a single, stable configuration: hence the mapping is equivalent to the one used above and the two-correlation method provides exactly the same results as our single-correlation function approach. The same holds in the second case, again provided the system potential V_s has a single stable point. Indeed, for an arbitrary V_s potential, the IO model is described by a T-independent spectral density. Hence, the spectral density can be obtained, for instance, at low enough T where the system dynamics is effectively Brownian HO, *i.e.* with the approach described in the main text. However, when

problem, where this condition follows from the requirement that no imaginary frequency appears among the eigenfrequencies of the whole system.

an exact mapping cannot be established, the method proposed above provides *one* IO model and memory kernel, namely the limiting one holding at low T, which is then supposed to work at higher temperatures. In this case, the above mentioned two-correlation function approach, when used with a 'guessed' conservative force, does provide a *different* memory kernel and corresponding IO model.

Appendix B: Anharmonic chain representation

In this Appendix it is shown how a simple exponential interaction model can be obtained by extending the linear chain representation of the bath [21–24, 28] to include anharmonic effects. The approach has the advantage of preserving the thermodynamic stability of the original IO Hamiltonian of Eq. (8) and of requiring just one representative length as a parameter. By thermodynamic stability we mean the existence of a ground state of the combined system for any reasonably well-behaved system potential $V(s)$, as it follows *e.g.* from $H \geq V_0$ when $V(s)$ is bound from below ($V \geq V_0$) and H is of the form given in Eq. 8.

The starting point is the effective mode transformation that brings the bath Hamiltonian of Eq. (8) in linear chain form [21–24]

$$H = \frac{p_s^2}{2m} + V(s) + \delta V(s) - \sum_{n=0}^{\infty} \bar{D}_n \bar{X}_n \bar{X}_{n+1} + \sum_{n=1}^{\infty} \left(\frac{\bar{P}_n^2}{2\mu} + \frac{\mu \Omega_n^2}{2} \bar{X}_n^2 \right) \tag{B1}$$

Here $\bar{X}_0 \equiv s$ and $\bar{X}_n$ are *unscaled* effective-mode coordinates with mass μ; correspondingly, $X_n = \bar{X}_n \sqrt{\mu}$ for $n = 1, 2, ..$ are the mass-scaled coordinates introduced in Ref. [23], and $\bar{D}_0 = \sqrt{\mu} D_0$, $\bar{D}_n = \mu D_n$ ($n \geq 1$) relate the coupling coefficients used here to those introduced in Ref. [23]. The effective mode parameters $\bar{D}_n$ and Ω_{n+1}^2 ($n = 0, 1, 2, ..$) are determined by the spectral density $J_n(\omega)$ describing the residual bath after the n^{th} effective mode has been introduced, and in turn all these quantities can be computed recursively using $J_0(\omega)$ only as input [23]. Furthermore, $\delta V(s)$ is the counter-term providing the thermodynamic stability of Eq. (8).

We first show that the Hamiltonian of Eq. (B1) can be re-expressed in order to make its stability evident, namely as

$$H = \frac{p_s^2}{2m} + V(s) + \sum_{n=1}^{\infty} \left\{ \frac{\bar{P}_n^2}{2\mu} + \frac{\mu \bar{\omega}_n^2}{2} \left(\bar{X}_n - \beta_n \bar{X}_{n-1} \right)^2 \right\} \tag{B2}$$

where $\beta_n = \bar{D}_{n-1} / \mu \bar{\omega}_n^2$ and $\bar{\omega}_n$ is a *renormalized* effective mode frequency,

$$\bar{\omega}_n^2 = \Omega_n^2 - \delta \Omega_n^2$$

Here the renormalization frequency is given by $\delta \Omega_n^2 \equiv \frac{2}{\pi} \int_0^\infty \frac{J_n(\omega)}{\omega} d\omega$, as usual [23]. In order to prove this, with the definition of β_n above, we only need to show that $\bar{\omega}_n^2 \equiv \frac{D_{n-1}^2}{\delta \Omega_{n-1}^2}$ holds, since Eq. (B2) is easily shown to reduce to Eq. (B1) under such circumstance. To see that this is indeed the case, we consider the fundamental propagators

$$W_n(z) = \frac{2}{\pi} \int_0^\infty \frac{J_n(\omega) d\omega}{\omega - z}$$

and their two-term recurrence relation

$$W_n(z) = \Omega_n^2 - z^2 - \frac{D_{n-1}}{W_{n-1}(z)}$$

and notice that $W_n(0) \equiv \delta \Omega_n^2$, hence

$$\Omega_n^2 - \delta \Omega_n^2 \equiv \bar{\omega}_n^2 = \frac{D_{n-1}}{\delta \Omega_{n-1}^2}$$

Next we modify the chain to introduce anharmonic effects in the dynamics of the first effective mode of the bath. This is accomplished by replacing the harmonic oscillator potential with a Morse potential having the same frequency,

$$H = \frac{p_s^2}{2m} + V(s) + \frac{\bar{P}_1^2}{2\mu} + D_e \left(e^{\alpha(\bar{X}_1 - \beta_1 s)} - 1 \right)^2 + H_{res} \tag{B3}$$

where $D_e = \mu \bar{\omega}_1^2 / 2\alpha^2$, α^{-1} is a characteristic length and

$$H_{res} = \sum_{n=2}^{\infty} \left\{ \frac{\bar{P}_n^2}{2\mu} + \frac{\mu \bar{\omega}_n^2}{2} \left(\bar{X}_n - \beta_n \bar{X}_{n-1} \right)^2 \right\}$$

is the residual bath. The Hamiltonian of Eq. (B3) contains an exponential system-bath coupling and reduces to the standard IO Hamiltonian for $\alpha \to 0$. For $s \approx 0$ it gives

$$H = H_S + H_{SB} + H_B$$

where H_S is the bare system Hamiltonian,

$$H_B = \frac{\bar{P}_1^2}{2\mu} + D_e \left(e^{\alpha \bar{X}_1} - 1 \right)^2 + H_{res}$$

is the modified (anharmonic) bath, and

$$H_{SB} = -\alpha^{-1} \bar{D}_0 e^{\alpha \bar{X}_1} \left(e^{\alpha \bar{X}_1} - 1 \right) s$$

Key words. Relaxation, quantum dynamics, spectral density, brownian motion.

References

[1] A. Nitzan, Chemical Dynamics in Condensed Phases - Relaxation, Transfer and Reactions in Condensed Molecular Systems, Oxford Graduate Texts (Oxford University Press, 2006).
[2] A. O. Caldeira and A. J. Leggett, Phys. Rev. A **31**, 1059–1066 (1985).
[3] G. W. Ford, J. T. Lewis, and R. F. O'Connell, Phys. Rev. A **37**, 4419–4428 (1988).
[4] U. Weiss Quantum Dissipative Systems, 3rd edition (World Scientific, Singapore, 2008).
[5] N. Pottier, Nonequilibrium statistical physics: linear irreversible processes, Oxford Graduate Texts (Oxford University Press, 2010).
[6] M. Nest and R. Kosloff, J. Chem. Phys. **127**(13), – (2007).
[7] H. D. Meyer, U. Manthe, and L. S. Cederbaum, Chem. Phys. Lett. **165**, 73–78 (1990).
[8] M. H. Beck, A. Jäckle, G. A. Worth, and H. D. Meyer, Phys. Rep. **324**, 1–105 (2000).
[9] H. D. Meyer, F. Gatti, and G. A. Worth (eds.), Multidimensional Quantum Dynamics: MCTDH Theory and Applications (Wiley-VCH, Weinheim, 2009).
[10] S. Valleau, A. Eisfeld, and A. Aspuru-Guzik, J. Chem. Phys. **137**(22), 224103 (2012).
[11] R. Zwanzig, Phys. Rev. **124**(Nov), 983–992 (1961).
[12] H. Mori, Prog. Theor. Phys. **33**(3), 423–455 (1965).
[13] S. D. Ivanov, F. Gottwald, and O. Kühn, ArXiv e-prints, http://arxiv.org/abs/1412.1688.
[14] R. Kubo, M. Toda, and N. Hashitsume, Statistical Physics II - Nonequilibrium Statistical Mechanics, Springer Series in Solid-State Sciences, Vol. 31 2nd ed. (Springer Verlag, 1991).
[15] M. Tuckerman and B. J. Berne, J. Chem. Phys. **98**(9), 7301 (1993).
[16] G. A. Worth, H. D. Meyer, and L. S. Cederbaum, J. Chem. Phys. **109**(9), 3518–3529 (1998).
[17] M. Nest and H. D. Meyer, J. Chem. Phys. **119**(1), 24–33 (2003).
[18] I. Burghardt, M. Nest, and G. A. Worth, J. Chem. Phys. **119**(11), 5364–5378 (2003).
[19] L. S. Cederbaum, E. Gindensperger, and I. Burghardt, Phys. Rev. Lett. **94**, 113003 (2005).
[20] M. Nest, Open system quantum dynamics with discretized environments, in: Multidimensional Quantum Dynamics: MCTDH Theory and Applications, edited by H. D. Meyer, F. Gatti, and G. A. Worth, (Wiley-VCH, 2009), chap. 22.
[21] K. H. Hughes, C. D. Christ, and I. Burghardt, J. Chem. Phys. **131**(2), 024109 (2009).
[22] K. H. Hughes, C. D. Christ, and I. Burghardt, J. Chem. Phys. **131**(12), 124108 (2009).
[23] R. Martinazzo, B. Vacchini, K. H. Hughes, and I. Burghardt, J. Chem. Phys. **134**(1), 011101 (2011).
[24] R. Martinazzo, K. H. Hughes, and I. Burghardt, Phys. Rev. E **84**, 030102(R) (2011).
[25] M. Bonfanti, G. F. Tantardini, K. H. Hughes, R. Martinazzo, and I. Burghardt, J. Phys. Chem. A **116**(46), 11406–11413 (2012).
[26] E. Vanden-Eijnden and G. Ciccotti, Chem. Phys. Lett. **429**(1–3), 310–316 (2006).
[27] G. A. Worth, M. H. Beck, A. Jäckle, and H. D. Meyer, The MCTDH Package, Version 8.2, (2000). H.-D. Meyer, Version 8.3 (2002), Version 8.4 (2007), Version 8.5 (2011). Current version: 8.5.3 (2013). See http://mctdh.uni-hd.de.
[28] M. P. Woods, R. Groux, A. W. Chin, S. F. Huelga, and M. B. Plenio, J. Math. Phys. **55**(3), 032101 (2014).